Ann. occup. Hyg., Vol. 49, No. 1, pp. 73–83, 2005

Published by Oxford University Press
doi:10.1093/annhyg/meh079

Applying Open-Path FTIR with Computed Tomography to Evaluate Personal Exposures. Part 2: Experimental Studies

CHANG-FU WU[1]*, MICHAEL G. YOST[1], RAM A. HASHMONAY[2] and TIMOTHY V. LARSON[3]

[1]Department of Environmental and Occupational Health Sciences, Box 357234, University of Washington, Seattle, WA 98195; [2]ARCADIS, PO Box 13109, Research Triangle Park, NC 27709 [3]Department of Civil and Environmental Engineering, Box 352700, University of Washington, Seattle, WA 98195, USA

Received 5 August 2003; in final form 19 August 2004; published online 13 December 2004

This paper presents the experimental evaluation results of using computed tomography coupled with OP-FTIR (CT-FTIR) measurement to estimate personal exposures. Experimental data were collected inside a ventilation chamber with a remote controlled robot as a surrogate for a real human. While the robot moved inside the chamber, a tracer gas (carbon monoxide) was released from a line source. A personal sampling device measured the true exposure on the robot. The estimated personal exposures were calculated from both the area sampling array data and the CT-FTIR measurements along with the information about the robot's locations in real time. The location information was obtained by applying image analysis on recorded digital videotapes.

The average slopes of the regression lines between the true and estimated exposures was 0.76 with 1 included in the 95% confidence interval. The concordance correlation factor (CCF) between the true and the CT-FTIR estimated exposures was 0.52, which was similar to the findings from previous simulation studies. Kriging the area sampling array data with an exponential algorithm instead of a liner algorithm improved the CCF value from 0.60 to 0.75. This suggests that using a different basis function for the SBFM algorithm might improve the performance of our estimation approach. Based on the sensitivity and specificity analysis of the experimental data, we demonstrated that this approach is suitable as a warning system.

Keywords: area monitors; computed tomography; open-path FTIR; optical remote sensing; personal exposure; radial plume mapping

INTRODUCTION

The most common way to evaluate personal exposures uses either sampling pumps with appropriate collecting media or passive sampling devices. Most of these devices cannot provide real-time information and are not suitable for evaluating short-term exposures. Some modern real-time monitors may provide real-time information *in situ*. However, they usually can only monitor certain types of air contaminants. Prior knowledge about the chemical properties of the existing gases or vapors is required in order to choose the right type of detectors. This information may not always be available.

*Author to whom correspondence should be addressed.
Fax: +1 206 543 8123; e-mail: cfwu@u.washington.edu

Unlike those personal monitors, open-path Fourier transform infrared (OP-FTIR) spectroscopy has some features that are useful for exposure assessments, such as identifying and quantifying mixtures of airborne compounds with low detection limits in real time (Levine *et al*., 1989; Yost *et al*., 1992). In the previous numerical simulation study (Wu *et al*., 2004), a companion paper, we demonstrated the feasibility of using computed tomography coupled with simulated OP-FTIR measurement (CT-FTIR) to estimate personal exposures. The next logical step is to collect experimental data to support these findings. Simulation studies cannot account for all the factors that can contribute to errors in estimating personal exposures. The chamber studies described here, conducted under controlled conditions, can help to

evaluate the actual performance of the proposed approach under more realistic conditions.

We conducted a series of experiments in an exposure chamber to evaluate work practices where workers move around a two-dimensional (2D) plane. The one-dimensional (1D) scenario in the simulation study (Wu *et al*., 2004) was not evaluated here. This is because the 1D scenario was used as a basic model to understand the theories behind the proposed approach for exposure estimation and had limited applications.

The goal of these 2D experiments is to evaluate the performance of CT-FTIR in estimating the 15 min TWA (time weighted average) personal exposures. We released a tracer gas from a line source inside a ventilation chamber to simulate plumes of pollutants residing in the air. The 15 min TWA exposures measured from a personal sampler were compared to the 15 min TWA values estimated from the CT-FTIR approach and from a real-time sensor array.

EXPERIMENTAL DESIGN

Chamber and OP-FTIR

The ventilation chamber is 11.1 m long, 5.4 m wide and 2.4 m high. The chamber has a push–pull configuration with an inlet and an outlet fan operated by a tandem adjustable frequency controller to provide plug-flow ventilation. Our OP-FTIR instrument is a custom-built unit by ETG (Environmental Technologies Group, Inc., Norcross, GA) based on a modified Nicolet (Nicolet Inst. Corp., Madison, WI) ST-1 optical bench. It has a liquid nitrogen cooled mercury-cadmium-telluride (MCT) detector and a unistatic design with the IR source, interferometer, and detector housed in one box. A remote retroreflector returns the external beam back over the same path to the spectrometer. The OP-FTIR instrument is mounted on a scanner that can direct the IR beam over 360° rotation and ±30° elevation, controlled by a Unidex stepper-motor computer controller (Aerotech, PA). The OP-FTIR system is operated through a MS-DOS PC with a Pentium 133 MHz processor. A detailed description about the chamber and the OP-FTIR instrument can be found in Wu *et al*. (1999).

Figure 1 shows the beam geometry for these experiments configured with nine corner-cube-type retroreflectors. This geometry is similar to that used in prior simulation studies (Wu *et al*., 2004). The OP-FTIR was positioned at the coordinate (0,0). Each beam scanned parallel to the floor with the optical centerline at a height of 1.45 m. There were no simultaneous signals from adjacent retroreflectors during sampling of any of the beam paths. This was verified by blocking the nearby retroreflectors with a piece of thick paper and observing that the strength of the IR signal for a certain beam path did not change.

Tracer gas and subject

The tracer gas used in the chamber study was carbon monoxide (CO). It was chosen for two reasons. First, CO has distinct absorption features in the FTIR spectra. Second, the NIOSH analytical method for CO uses a measurement technique based on electrochemical sensors. Usually these sensors are small and relatively inexpensive, and can provide real-time information. These features allow us to collect simultaneous area and personal samples in the chamber.

To create a CO plume in the chamber, a mixture of 10% CO with nitrogen was released from a line source hanging vertically from the ceiling. The line source was a 0.5 m long soaker hose with a diameter of 0.6 cm (1/4 in.). It was located 1.5 m above the floor and the flow rate was controlled by a mass flow controller (Sierra Instruments, Inc., Monterey, CA). Experiments were conducted at three different release locations (Fig. 1).

Human subjects were not involved in this study as initially there were some concerns over routinely exposing people to CO, since it is potentially an asphyxiating agent. Instead, a remote-controlled robot was used as a surrogate for real human subjects. The robot was modified from the K'NEX® Control-A-Bot (Hatfield, PA) to an adolescent-sized robot with a height of 1.53 m. The remote controller was modified so that it could be connected to a personal computer through a CYREL16 electromechanical relay board (CyberResearch, Inc., Branford, CT). A program written in the MS Visual Basic® (Microsoft Corporation, Redmond, WA) was used to operate the remote controller.

Sampling system

The personal sampling device used in this study was a 3ME/F CO CiTiceL® electrochemical sensor (City Technology Ltd., Portsmouth, UK). The sensor came with a circular printed circuit board (PCB) that converts the microamp level output signal from the sensor to a milivolt level signal. Connection to the sensor was through a four-pin socket, two for the power supply and two for the output signal. Calibration can be done through the built-in span and zero potentiometers. Two 9 V batteries were connected to the sensor as the power source. The output milivolt signal was amplified by a Universal Single Ended Amplifier (EME Systems, Berkeley, CA) and then sent to a portable HOBO® datalogger (Onset Computer Corporation, Bourne, MA) which has a built-in temperature sensor. A mounting collar and a push-in plug from the City Technology Ltd. were mounted on the sensor. One end of a 15 cm long Tygon tube was connected to the air inlet of the push-in plug and the other end was taped near the robot's nose (at a height of 1.45 m). The air outlet of the push-in plug was connected to a personal sampling pump.

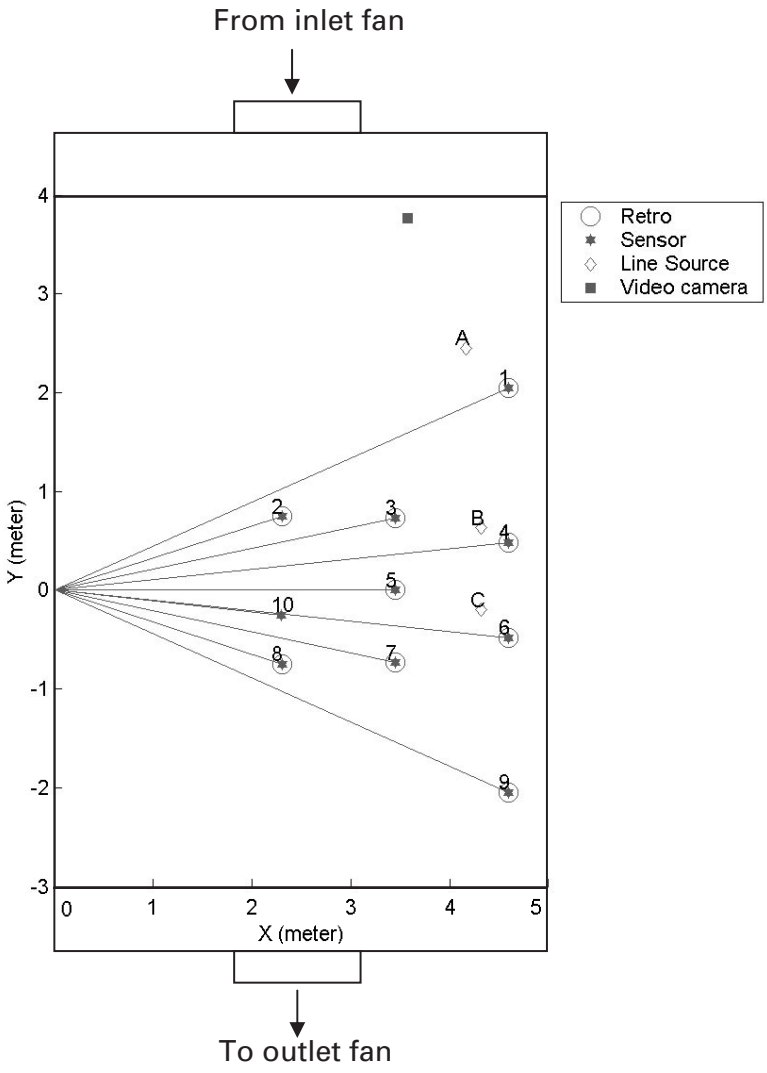

Fig. 1. Top view of the experimental setup. OP-FTIR was located at (0,0). The nine retroreflectors and ten electrochemical sensors were placed at the same height of 1.45 m. The ◇ symbols represent the three different release locations for the tracer gas. The video camera was positioned 2.25 m above the floor.

The pump drew air continuously at a flow rate of 150 ml/min to ensure that enough air passed across the CO sensor.

An area sampling array, consisting of 10 identical CO CiTiceL® electrochemical sensors, was built inside the chamber. These sensors are small (diameter: 43 mm, thickness: 31 mm) and so have minimal effects on the airflow. This area sampling array is used to confirm the performance of the CT-FTIR approach. Figure 1 shows the sensors' locations. One sensor was attached to each of the retroreflectors. An additional sensor (#10) was positioned between sensors #2 and #8. All the sensors had the push-in plugs described above. Air was drawn continuously across each of the CO sensors through polyethylene tubing at a flow rate of 150 ml/min. The inlets of the CO sensors were positioned at the same height (1.45 m) as the inlets of the personal sampling train and the OP-FTIR's scanning domain. Two rechargeable Ni-MH battery packs were used as the power supply for all the sensors. The milivolt output signals were connected to an ATDAQ® 1411 data acquisition board (CyberResearch, Inc., Branford, CT) on a personal computer. The data acquisition board has 16 single-ended channels and can covert analog voltage signal to digital signal. The maximum sampling rate is 100kHz and the resolution is 12 bits. A program written in the MS Visual Basic® was used to collect the data from the area sampling array.

Calibration

The outputs of electrochemical sensors can vary with temperature. To compensate for any temperature effect, each sensor was calibrated against zero gas and

400 ppm span gas at 13°C (room temperature) and 0°C (inside a refrigerator). The calibration curve at a certain temperature can be obtained by using the temperature compensated milivolt signals at 0 and 400 ppm. On average, the output signal was ~1 mV/ppm. The OP-FTIR was calibrated against the electrochemical sensors by conducting two homogeneous concentration chamber experiments (Hashmonay *et al*., 1998) where both OP-FTIR and point samples were taken. For the first experiment, the average concentration measured by the OP-FTIR and the electrochemical sensors was 7.3 and 7.2 ppm (with a spatial standard deviation (SD) of 0.7 ppm), respectively. For the second experiment, the average concentration measured by the OP-FTIR and the electrochemical sensors was 14.5 and 14.2 ppm (SD = 0.8 ppm), respectively. This indicated that the two measuring methods were comparable. Detailed description of the calibration experiments can be found in Wu (2002).

Tracking system

To estimate the robot's exposure levels from either the OP-FTIR measurements or the area sampling array, we need to know the robot's location in real time. This was done by analyzing the recorded video frames from a digital video camera. The location of the video camera is shown in Fig. 1. Detailed description about this tracking system was presented in Wu (2002). Briefly, a red and a blue color marker were placed on the robot's right and left feet, respectively. A computer program written in Matlab® (The Mathworks, Inc., Natick, MA) was used to track the color markers on the video frames. We placed ten yellow brackets on the floor (at the same height as the color markers) as spatial reference points. We then applied the theory of perspective geometry to transform the robot's coordinates on the 2D images to the robot's locations in the real world. From a previous validation experiment (Wu, 2002) conducted inside the ventilation chamber, we determined that the average root-mean-square (RMS) error of this tracking system was ~0.06 m.

Data acquisition

Thirteen experiments were conducted inside the chamber, each lasting 15 min. The CO release rate was varied between 0.4 and 3.2 l/min and the fan speed was varied between 9 and 18 Hz. The CO release location, release rate, and fan speed were fixed for each of the experiments (Table 1). The average air flow rates inside the chamber for a fan speed set at 9 and 18 Hz were 35.1 and 69.3 m^3/min, respectively. These values were obtained from a mass-balance calculation using the CO release rate and the average measured CO concentration levels from the point samples. By varying the line source location, CO release rate, and the fan speed, we expected to create plumes with different size and concentrations.

In each experiment, the robot moved within the OP-FTIR scanning region in a rectangular pattern. While the robot moved inside the chamber for 15 min, four different kinds of data were collected simultaneously: (i) Personal samples were collected with the electrochemical sensor on the robot. The HOBO datalogger recorded the milivolt signals from the CO sensor and the temperature reading from the HOBO's built-in temperature sensor every second. After each

Table 1. Summary table of the experiments

Experimental setup			15 min Exposure level				SBFM endpoint	
Release location	Fan speed Hz	Release rate l/min	$C_{TWArobot}$[a] ppm	$C_{TWAkrig}$[b] ppm	$C_{TWAgauss}$[b] ppm	$C_{TWAftir}$[b] ppm	$\overline{CCF}_{gauss}$[c]	$\overline{CCF}_{PIC}$[d]
A	18	0.4	4.7	9.0	8.0	9.1	0.94	0.95
	18	0.8	6.6	13.8	13.1	12.1	0.96	0.96
	18	1.6	8.6	18.9	17.5	22.1	0.97	0.93
	18	1.6	7.0	10.9	11.2	11.3	0.87	0.93
	18	2.4	12.0	28.9	24.0	20.9	0.98	0.92
	18	3.2	15.7	30.5	32.5	38.8	0.97	0.89
B	9	0.8	16.0	16.8	17.2	16.6	0.97	0.92
	9	1.6	14.8	17.8	18.1	20.8	0.86	0.93
	9	3.2	20.6	39.1	47.3	31.9	0.91	0.88
	12	0.8	6.3	7.2	8.6	7.8	0.84	0.99
	12	1.6	5.5	8.2	8.8	8.8	0.73	0.88
C	9	0.8	12.3	16.8	17.5	26.1	0.99	0.92
	9	1.6	7.7	8.1	8.4	17.0	0.87	0.87

[a]The robot's 15 min TWA exposures measured from the personal sampling device.
[b]The robot's 15 min TWA exposures estimated from the area samplers and CT-FTIR.
[c]The average CCF values between the measured and predicted values at the point samplers' locations by fitting a Gaussian function directly to the sampling array data.
[d]The average CCF values between the measured and predicted PICs from the SBFM reconstruction.

experiment, the data were downloaded into a personal computer. (ii) The OP-FTIR scanned the nine retroreflectors sequentially and repeatedly using the beam geometry shown in Fig. 1. Each sweep of the nine beam paths requires 98 s and there were approximately nine sweeps for the 15 min time period. (iii) The area sampling array continuously measured the CO concentrations. Data collection software written in MS Visual Basic® recorded the digitized signals as fast as possible and saved the one-second average values for the entire 15 min period as a text file on a personal computer. (iv) The digital video camera recorded the robot's locations on a miniDV tape. After the experiments, the video images were captured with a PCI FireWrie (IEEE 1394) card and saved as audio–video interleave (AVI) files with a one frame per second (fps) resolution on a personal computer.

Each OP-FTIR spectrum was collected at 2 cm^{-1} spectral resolution by the Nicolet PC/IR™ software. Each day before the experiments, a clean spectrum for each beam path was collected. These clean single-beam spectra collected on different days were ratioed to each other. The cleanest set of single-beam spectra at the quantification region (described below) was used as the background spectra. The collected sample spectra were quantified by classical least squares method (Haaland and Easterling, 1982) using the Nicolet OMNIC® TQ Analyst with OMNIC® Macro for automating the quantification process. The spectral range used for CO quantification was 2050–2220 cm^{-1} (Esler *et al*., 2000). Since nitrous oxide (N_2O) has absorption feature in this region, it also is included in the quantification procedure. The reference spectra for quantification (2 cm^{-1} resolution) were obtained from the EXAMS library (Expert Air Monitoring System, Automotive Safety and Health Research, General Motors Corporation). The quantification method used two reference spectra at 493 and 202 ppm-m for CO and one reference spectrum at 336 ppm-m for N_2O.

DATA ANALYSIS

The milivolt signals from the personal sampler and the area sampling array were converted to ppm. values using the calibration curves described in the previous section. The calibration curves were temperature adjusted based on the temperature readings recorded by the HOBO datalogger. The 15 min TWA for CO personal exposure at the mth experiment ($C_{\mathrm{TWArobot},m}$) were calculated as:

$$C_{\mathrm{TWArobot},m} = \frac{1}{T}\sum_{t=1}^{T} C_{\mathrm{robot},t,m} \qquad (1)$$

where $C_{\mathrm{robot},t,m}$ is the ppm value obtained from the electrochemical sensor on the robot at time t (t = 1–900); m is the experiment index, and T is the total sampling time (=900 s).

To estimate the personal exposure from the area sampling array, two approaches were applied. The first approach used the kriging method to create a concentration map from the area sampling array every second. The kriged maps were created with a linear algorithm using the GLOBEC Kriging Software Package (U.S. GLOBEC Georges Bank Program, Woods Hole Oceanographic Institution, Woods Hole, MA) under the Matlab computing environment. The 15 min TWA personal exposure at the mth experiment estimated from this approach ($C_{\mathrm{TWAkrig},m}$) were calculated as:

$$C_{\mathrm{TWAkrig},m} = \frac{1}{T}\sum_{t=1}^{T} C_{\mathrm{krig},m,t}\left(x_{\mathrm{robot},t,m}, y_{\mathrm{robot},t,m}\right) \qquad (2)$$

where $C_{\mathrm{krig},m,t}$ is the CO concentration map created by kriging the 10 area samplers at time t at the mth experiment assuming a linear function; $x_{\mathrm{robot},t,m}$ and $y_{\mathrm{robot},t,m}$ are the x and y coordinates of the robot's location at time t at the mth experiment, respectively; and $C_{\mathrm{krig},m,t}(x_{\mathrm{robot},t,m}, y_{\mathrm{robot},t,m})$ is the concentration value at point location $x_{\mathrm{robot},t,m}$ and $y_{\mathrm{robot},t,m}$ on the $C_{\mathrm{krig},m,t}$ map.

The second approach was the fitting of a single-mode bivariate Gaussian model directly to the data obtained from the sampling array. The fitting algorithm was similar to the SBFM (Smooth Basis Function Minimization) algorithm described in prior simulation studies (Wu *et al*., 2004). The error function for minimization at time t at the mth experiment in the fitting procedure was the sum of squared errors ($SSE_{\mathrm{arrayGauss},t,m}$), defined as follows:

$$SSE_{\mathrm{arrayGauss},t,m} = \sum_{n}\left(C_{\mathrm{sensor\_observed},n,t,m} - C_{\mathrm{sensor\_predicted},n,t,m}\right)^2 \qquad (3)$$

where n is the sensor number index (n = 1–10); $C_{\mathrm{sensor\_observed},n,t,m}$ is the observed concentration obtained from the nth sensor at time t at the mth experiment; and $C_{\mathrm{sensor\_predicted},n,t,m}$ is the corresponding predicted concentration adjusted at the minimization procedure to minimize the SSE and was defined as:

$$C_{\mathrm{sensor\_predicted},n,t,m} = G_{\mathrm{sensor}}\left(x_{\mathrm{sensor},n}, y_{\mathrm{sensor},n}; p_{\mathrm{sensor},t,m}\right) \qquad (4)$$

where G_{sensor} is the density function of the bivariate Gaussian; $p_{\mathrm{sensor},t,m}$ is the parameter vector with six elements for the Gaussian density function at time t at the mth experiment; $x_{\mathrm{sensor},n}$ and $y_{\mathrm{sensor},n}$ are the x and y coordinates of the nth sensor's location. The six parameters for the Gaussian function are: the peak location (μ_x,μ_y), two standard deviations (σ_x,σ_y), the peak height (h), and the correlation coefficient (ρ). The concordance correlation factor (CCF) (Fisher and Van Belle, 1993; Hashmonay *et al*., 1999) between

the paired $C_{\text{sensor\_observed}}$ and the $C_{\text{sesnor\_predicted}}$ for each map (named CCF_{gauss}) was calculated as a summary measure to determine if the SBFM algorithm reached a good solution. The CCF is similar to the Pearson correlation coefficient with adjustment for location and scale shifts. The CCF values are bounded between -1 and 1. The 15 min TWA personal exposure at the mth experiment estimated from the second approach ($C_{\text{TWAgauss},m}$) were calculated as:

$$C_{\text{TWAgauss},m} = \frac{1}{T}\sum_{t=1}^{T} G_{\text{sensor}}\left(x_{\text{robot},t,m}, y_{\text{robot},t,m}, p_{\text{sensor},t,m}\right) \quad (5)$$

In addition to evaluating the 15 min TWA values, we compared these two approaches on a mapping basis. The rectangular area where the robot moved around was overlapped with a 6×11 grid system having a grid size of 0.5 m. Every second, the $p_{\text{sensor},t,m}$ parameter vector in equation 4 was applied with the one-mode bivariate Gaussian density function to calculate a Gaussian-fitted map based on the above grid system. The kriged map $C_{\text{krig},m,t}$ in equation 2 was assumed to be the corresponding 'true' map. By the end of each experiment, there were 900 pairs of true and Gaussian-fitted maps. We calculated the CCF values (called $\text{CCF}_{\text{GaussKrigPoint}}$) for each pair of maps. The mean of the 900 $\text{CCF}_{\text{GaussKrigPoint}}$ values (called $\overline{\text{CCF}}_{\text{GaussKrigPoint}}$) was used to determine the agreement between the true and Gaussian-fitted maps with a 1 s temporal resolution. We also calculated the CCF value (called $\text{CCF}_{\text{GaussKrigMean}}$) between the mean maps of the 900 true maps and the 900 Gaussian-fitted maps. The $\text{CCF}_{\text{GaussKrigMean}}$ represented the time-weighted agreement between the true and Gaussian-fitted maps for each experiment.

To estimate personal exposures from the OP-FTIR measurements, the CT-FTIR approach was applied here. This approach used the SBFM algorithm to reconstruct a single-mode bivariate Gaussian plume from the PIC data (path integrated concentration; the OP-FTIR measurements). The error function for minimization was the sum of squared errors of the observed PIC ($\text{PIC}_{\text{observed}}$) and the predicted PIC ($\text{PIC}_{\text{predicted}}$). A detailed description of this approach can be found in Wu *et al*. (2004). To obtain one reconstruction, we employed nine observed PICs (one from each of the nine rays). We applied running average PIC (PICrun) updating strategy investigated in the simulation studies by Wu *et al*. (2004). Under this updating strategy, approximately every 10.9 s (98 s per sweep/9 rays) the oldest PIC was updated with the latest PIC and the other eight PICs were unchanged. The nine PICs were updated completely every 98 s. Each experiment produced 83 reconstructions (900 s/10.9 s), generating 83 Gaussian parameter vectors. The CCF value between the paired $\text{PIC}_{\text{observed}}$ and the $\text{PIC}_{\text{predicted}}$ for each reconstruction (named CCF_{PIC}) was calculated as an indicator for determining if the minimization procedure reached a solution. The 15 min TWA personal exposure at the mth experiment estimated from this approach ($C_{\text{TWAftir},m}$) was calculated as:

$$C_{\text{TWAftir},m} = \frac{1}{T}\sum_{t=1}^{T} G_{\text{ftir}}\left(x_{\text{robot},t,m}, y_{\text{robot},t,m}, p_{\text{ftir},t,m}\right) \quad (6)$$

where $p_{\text{ftir},t,m}$ is the Gaussian parameter vector that was obtained from the SBFM reconstruction for the set of nine PICs with the latest PIC collected right before time t at the mth experiment. The $x_{\text{robot},t,m}$ and $y_{\text{robot},t,m}$ in equation 6 are the robot's average locations during the period when the last PIC was collected, similar to the W10sec updating strategy described in the simulation studies by Wu *et al*. (2004).

We evaluated the quality of the CT-FTIR reconstructed maps by comparing them to the kriged maps from the area samplers. For each CT-FTIR reconstructed map, it was assumed that the corresponding true map was the mean map of those 1 s kriged maps, obtained during the same reconstruction period. For each experiment, we have 83 pairs of reconstructed and true maps. We calculated the CCF value (called $\text{CCF}_{\text{CTKrigPoint}}$) for each pair of maps. The mean of the 83 $\text{CCF}_{\text{CTKrigPoint}}$ values (called $\overline{\text{CCF}}_{\text{CTKrigPoint}}$) was used to determine the agreement between the true and CT-FTIR reconstructed maps with an average temporal resolution of 10.9 s. We also calculated the CCF value (called $\text{CCF}_{\text{CTKrigMean}}$) between the mean maps of the 83 true maps and the 83 CT-FTIR reconstructed maps. The $\text{CCF}_{\text{CTKrigMean}}$ represented the time-weighted agreement between the true and CT-FTIR reconstructed maps for each experiment.

A regression model was applied for the exposure data analysis:

$$\log(C_{\text{TWArobot}}) = \textit{intercept} + \beta_1 \log(C_{\text{TWAestimate}}) \quad (7)$$

where $C_{\text{TWAestimate}}$ is the 15 min TWA exposure level estimated either from the area sampling array (C_{TWAkrig} and C_{TWAgauss}) or from the CT-FTIR (C_{TWAftir}). Since C_{TWArobot} and $C_{\text{TWAestimate}}$ were estimated from paired samples, we did not include the experimental settings (e.g. the source location and fan speed) as covariates in the model. We also fitted analogous untransformed models, but decided to use only the log-transformed model. The residual plots showed that log transforming the measurements helped to improve the assumption of equal variance. Two parameters were used to determine the performance of our estimation approach: the slope and CCF (named CCF_{TWA}) between C_{TWArobot} and

$C_{TWAestimate}$. Ideally, we would like to have the slope and the CCF_{TWA} equal to one.

RESULTS AND DISCUSSION

The robot's 15 min TWA exposure levels in the 13 experiments range from 4.7 to 20.6 ppm with a mean of 10.6 ppm (Table 1). The mean CCF_{gauss} and CCF_{PIC} values for all the experiments are high (>0.7), indicating that the fitting algorithm reached a good solution during the minimization process both for the point samples and the FTIR measurements.

Table 2 summarizes the regression modeling results with data from different estimation approaches. All the three regression lines have fitted R^2 >0.7. The empirical regression line using $C_{TWAkrig}$ as the predictor (Fig. 2) is:

$$\log(C_{TWArobot}) = 0.12 + 0.73^{*}\log(C_{TWAkrig}) \quad (8)$$

The slope is <1, meaning $C_{TWAkring}$ overestimated the true exposure level. The intercept term is not statistically significant under the log scale (Table 2). The regression lines using $C_{TWAgauss}$ and $C_{TWAftir}$ as the predictor are shown in Fig. 2. Both the regression lines also have slopes <1 and the intercepts terms are not statistically significant (Table 2). All three estimation approaches overestimated the true exposure levels (although the standard errors were relatively large and the 95% confidence intervals (CIs) just barely contained 1). One of the explanations for this overestimation is that the linear function in the C_{krig} (equation 2) or Gaussian function in the G_{sensor} (equation 5) and G_{ftir} (equation 6) 'over-smooth' the gradient of the concentration maps and may not reflect the true test condition. To test this hypothesis, we used an exponential algorithm during the kriging process and found that the slope between $C_{TWArobot}$ and $C_{TWAkrig}$ increased from 0.73 to 0.78.

In the previously simulation studies (Wu *et al*., 2004) we found that the plumes' size is a significant factor for predicting the true 15 min TWA. We attempted to verify this from the experimental data by calculating the mean of the 900 RMS values of the two standard deviations (σ_x, σ_y) in the $p_{sensor,t,m}$ vector and incorporating this variable in the regression model. However, because the plumes' size changed all the time, even within each experiment, we could not see its effect in predicting the personal exposures. Unless we have a more stable plume for each experiment, it probably would be difficult to observe this effect from the experimental data. In the real world, the plumes' size is also likely to be highly variable, as in these experiments. In addition to estimates of true exposure levels, we also can focus on the 'relative' exposure levels. For example, one might want to know if a worker at one working condition has higher exposure than at another condition. In this case, we are less concerned about the slope of our regression model, but more interested in the correlation between the true and estimated 15-min TWA values. This correlation was first tested by comparing the CCF_{TWA} values shown in Table 2. In the previous 2D simulation studies (Wu *et al*., 2004), we obtained CCF values that ranged between 0.50 and 0.58 from the CT-FTIR estimations. The CCF_{TWA} for $C_{TWAftir}$ was 0.52, which agrees well with the results from the simulation studies. The CCF_{TWA} for point sampling arrays ($C_{TWAkrig}$, $C_{TWAgauss}$) were at a similar level. We would expect the estimates from the point sampling array to have much better agreement with the $C_{TWArobot}$ since all 10 point samplers provide real time data while the CT-FTIR only can update the reconstruction every 10 s. However, they do not show much improvement. This might be because of the fact that we have only 10 point samplers inside the chamber and do not have enough spatial resolution to map the true concentration distribution. There are many different ways to describe how the concentration gradient changed from one sampling point to another. The use of an exponential algorithm during the kriging process improved the $CCF_{TWAkrig}$ from 0.60 to 0.75.

Besides using the CCF_{TWA} values to assess the correlation between $C_{TWArobot}$ and $C_{TWAestimate}$, we also calculated the Spearman correlation coefficient (Table 2). Being a nonparametric measure, it is not limited by some assumptions used in parametric

Table 2. Results from the regression models and correlation between measured and estimated C_{TWA}

Predictors	Regression model					Correlation	
	Intercept	SE[a]	β_1[b]	SE[a]	R^2	CCF_{TWA}[c]	Spearman[d]
$\log(C_{TWAkrig})$	0.12	0.17	0.73	0.14	0.72	0.60	0.78
$\log(C_{TWAgauss})$	0.08	0.14	0.76	0.12	0.79	0.62	0.84
$\log(C_{TWAftir})$	0.01	0.18	0.80	0.14	0.74	0.52	0.81

The dependent variable for the regression model is the log-transformed exposures measured by the electrochemical sensor on the robot.
[a]standard errors.
[b]coefficient for $\log(C_{TWAestimate})$.
[c]CCF values between $\log(C_{TWAestimate})$ and $\log(C_{TWArobot})$.
[d]Spearman's rank correlation coefficient between $\log(C_{TWAestimate})$ and $\log(C_{TWArobot})$.

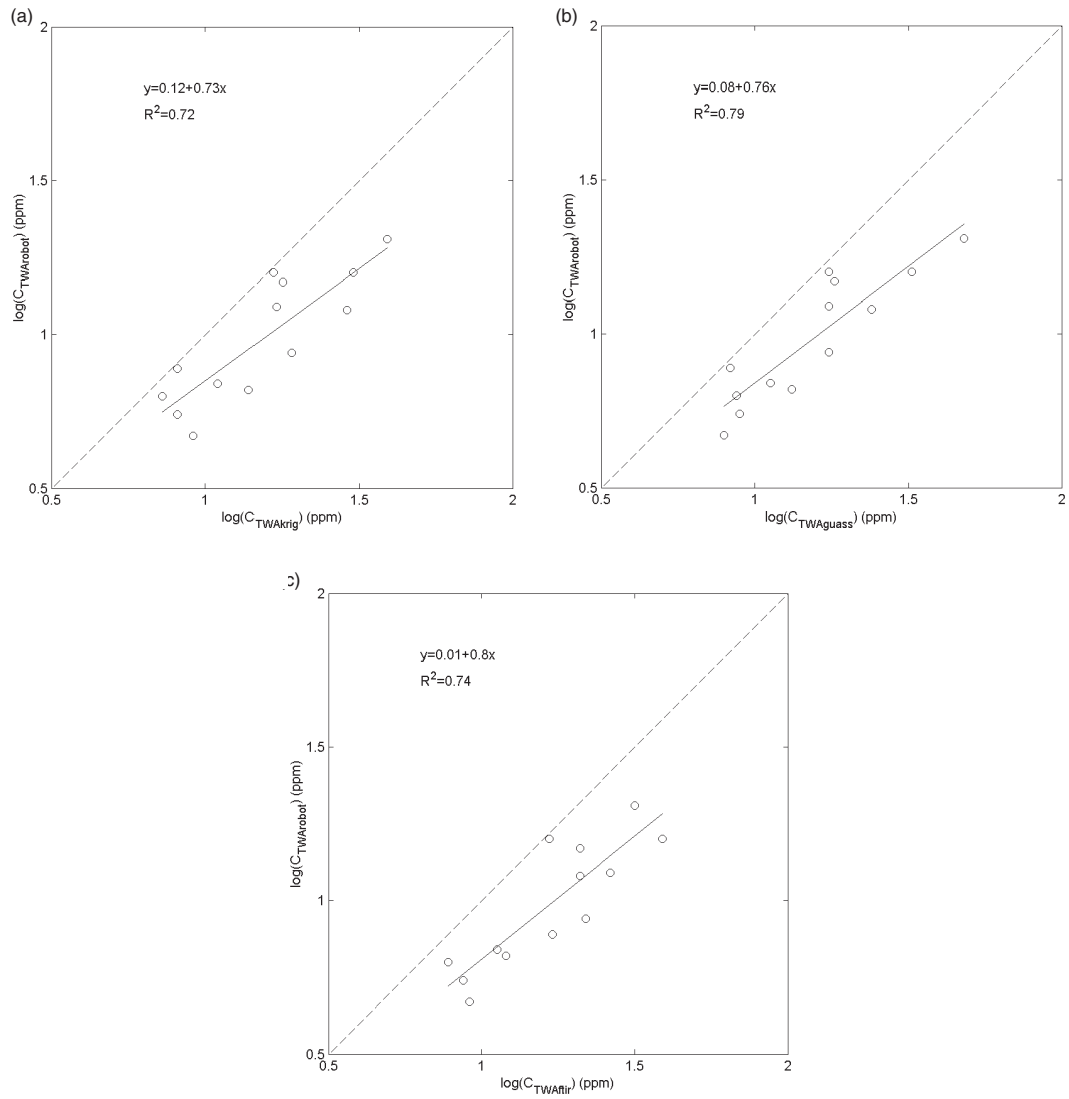

Fig. 2. Results from the regression model building process. The *y*-axis represents the robot's exposures measured from the personal sampling device. (a) The *x*-axis represents the estimated exposure levels calculated from kriging the sampling array data. (b) The *x*-axis represents the estimated exposure levels calculated from fitting a Gaussian function directly to the sampling array data. (c) The *x*-axis represents the estimated exposure levels calculated from the CT-FTIR approach.

regression models. The Spearman correlation coefficients are ∼0.8 for all the three estimation approaches tested in our experiment. This confirms the reasonably good CCF_{TWA} values found above and suggests that we can use these approaches to estimate the 'relative' exposure.

This idea can be simplified further to a binary (yes/no) exposure scenario, in which we use the estimation approaches as a screening tool to determine if a subject is above or below a certain exposure limit. In the field of epidemiology, the validity of a screening tool is measured by the sensitivity and specificity (Hennekens *et al.*, 1987). Sensitivity is defined as the probability of testing positive (i.e. estimating that the subject has exposure higher than the STEL) if the condition is truly present (i.e. the subject truly has exposure higher than the STEL). Specificity is defined as the probability of screening negative if the condition is truly absent. Ideally, we would like to have sensitivity and specificity close to 1. Figure 3 shows the results from the three estimation approaches assuming different exposure limits or warning limits. All the estimation approaches provide good sensitivity (=1) at different exposure limits due to overestimation of $C_{TWAkrig}$, $C_{TWAgauss}$ and $C_{TWAftir}$. From the viewpoint of protecting workers, this is an encouraging result, since we can successfully identify the conditions in which the subject has exposure higher than the exposure limit. Although the specificity generally increases when we set the exposure limit higher, the value (∼0.6) at the plateau region of the specificity curve is more representative

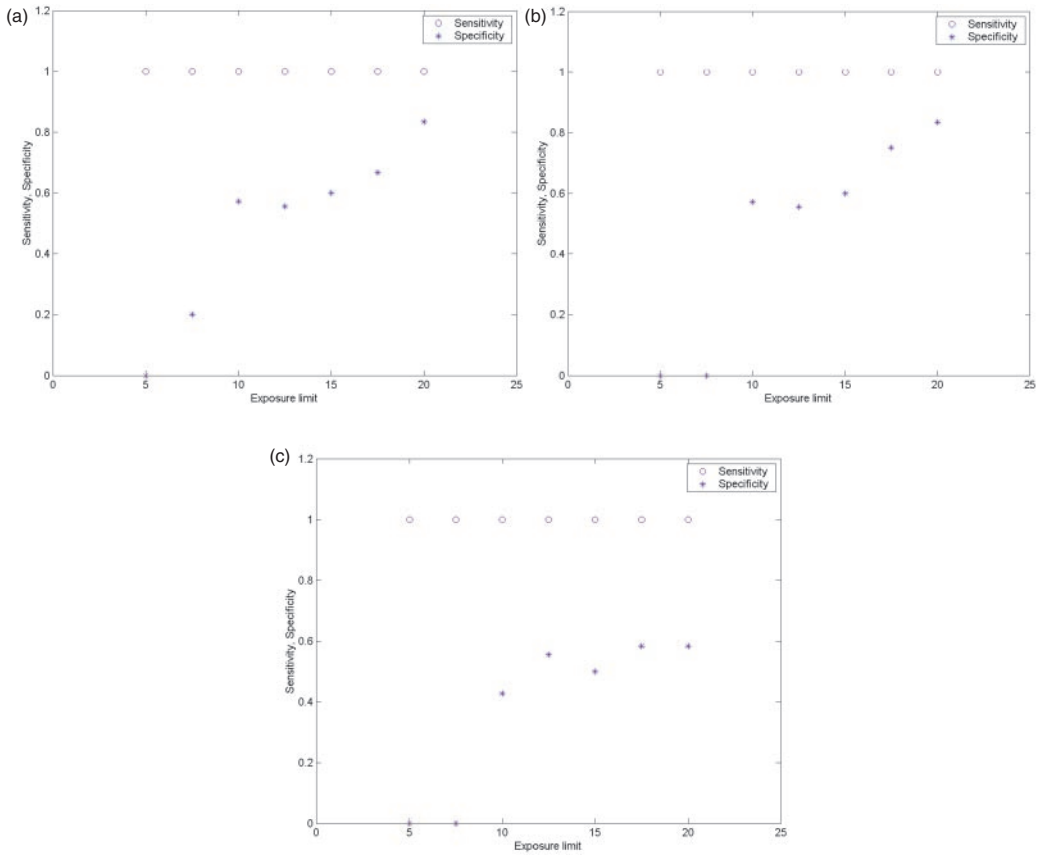

Fig. 3. Validity test for using different estimation approaches as screening tools. The x-axis represents the assigned exposure limit or warning limit. The *y*-axis represents the sensitivity and specificity. (a) $C_{TWAkrig}$. (b) $C_{TWAgauss}$. (c) $C_{TWAftir}$.

since that is where we have most of the data. The implications of this analysis are that a warning system using this CT-FTIR approach would be likely to prevent true overexposures, but may be prone to producing false alarms when the exposure limits are very low.

Table 3 summarizes the comparison results on a mapping basis among the three different analysis approaches (i.e. kriged maps, Gaussian-fitted maps and CT-FTIR reconstructed maps). The mean $\overline{CCF}_{GaussKrigPoint}$ ranged from 0.44 to 0.79, suggesting that there is still room for improvement by fitting functions other than the Gaussian model. Unlike what we found in the simulation studies for the PIC data (Wu *et al*., 2004), the time-weighted averaging process did not necessarily make the $CCF_{GaussKrigMean}$ higher than the $\overline{CCF}_{GaussKrigPoint}$. This probably occurs because the Gaussian-fitted maps have the same temporal resolution (1 s) as the kriged maps. On the contrary, since each PIC required ~10.9 s to be updated, the time-weighted averaging process made the $CCF_{CTKrigMean}$ higher than the $\overline{CCF}_{CTKrigPoint}$ for most of the experiments. In the simulation studies, the CCF_{TWA} lies between the $\overline{CCF}_{CT}$ (analogous to the $\overline{CCF}_{CTKrigPoint}$ in this study) and CCF_{CTmean} (analogous to the $CCF_{CTKrigMean}$ in this study). This is not always true in the chamber experiments. One explanation is that we know what the true map is in the simulation studies. However, for the experimental data, we can only assume that the kriged map is the true map. It is possible that the point samplers do not have enough spatial resolution to map the true distributions (as discussed above).

It was determined from a validation experiment (Wu, 2002) that the RMS error of our tracking system was 0.06 m. To verify if this error level was acceptable, we conducted a sensitivity analysis on the robot's location. Random noises at different orders of magnitude (two to ten times) of this RMS error level were added to the robot's location. The estimated 15 min TWA were recalculated. It was found that the CCF_{TWA} from all the three estimation approaches changed <0.07 even with random noise at levels up to 10 times of this RMS error. This suggests that discrepancy between the true and estimated C_{TWA} derives mainly from the mapping errors (i.e. difference between the true and estimated concentration maps) rather than tracking errors.

The CCF_{TWA} value (0.52) of the experimental studies obtained from the CT-FTIR estimation approach is compatible with the one obtained in the previous

Table 3. Comparison results on a mapping basis among the different reconstruction approaches

Exp. index	$\overline{CCF}_{GaussKrigPoint}$[a]	$CCF_{GaussKrigMean}$[b]	$\overline{CCF}_{CTKrigPoint}$[c]	$CCF_{CTKrigMean}$[d]
1	0.56	0.56	0.28	0.40
2	0.59	0.59	0.30	0.53
3	0.55	0.55	0.35	0.62
4	0.69	0.66	0.19	0.40
5	0.58	0.58	0.41	0.68
6	0.44	0.45	0.36	0.44
7	0.73	0.79	0.49	0.68
8	0.67	0.76	0.49	0.81
9	0.60	0.65	0.16	0.12
10	0.76	0.81	0.22	0.39
11	0.60	0.68	0.37	0.64
12	0.79	0.84	0.45	0.81
13	0.69	0.69	0.29	0.35

[a]The mean of the CCF values between the Gaussian-fitted and the kriged maps.
[b]The CCF value between the mean maps of the Gaussian-fitted maps and the kriged maps.
[c]The mean of the CCF values between the CT-FTIR reconstructed maps and the kriged maps.
[d]The CCF value between the mean maps of the CT-FTIR reconstructed maps and the kriged maps.

simulation studies by Wu *et al*. (2004). This suggests that the experimental study is a legitimate validation study to the simulation results. Based on the simulation results, we also can conclude that it is possible to improve the CCF_{TWA} values significantly if the OP-FTIR can scan the retroreflectors on a much faster time scale (i.e. being able to apply the concurrent PIC updating strategy introduced in the simulation studies).

To improve estimation from the CT-FTIR measurements, several potential approaches are discussed here. First, since kriging the area sampling array data with an exponential algorithm did improve the $CCF_{TWAkrig}$, we could apply several different basis functions to the SBFM algorithm during the reconstruction process. We could build a library of basis functions and choose the function that gives the best CCF_{PIC} value as the final basis function. Second, we might be able to fit or krig the OP-FTIR data directly in the PIC domain. The estimated concentration map can be obtained by calculating the derivative of the fitted PIC map. This approach has been tested in the 1D scenario by Wu *et al*. (2003). Third, we could also use another pixel-based CT algorithm for our radial scanning geometry as described by Hashmonay (2001). The maximum pixel number is the OP-FTIR ray number (i.e. 9). This pixel based approach may provide more flexibility than the function based SBFM algorithm.

There are several limitations in the current study. First, we have only 13 paired 15 min TWA values. This small sample size partially explained the relatively large standard errors for the intercepts and slopes of our models. Second, we arbitrarily chose a linear and an exponential algorithm for kriging the point sample data collected from the area array. To obtain more robust and unbiased kriging results, we would need to study the semivariogram of the electrochemical sensor measurements to determine the best models and coefficients. However, since we had 11,700 semivariograms (13 experiments $*$ 900 semivariograms per experiment) in the CT-FTIR experiments, we would need to develop a robust method to automate the choice of the right kriging algorithm and coefficients. Third, the subject used in this study was a robot and one can always argue that robot is not representative of a human. The robot did not breathe and did not dispense heat as a real person does. We did not simulate how a real person moves his/her hands and rotates the upper body while walking. The purpose of this study is to test whether the proposed estimation approaches have the potential to evaluate personal exposures. Our results suggest that it is worthwhile to conduct more studies on this topic and consider recruiting human subjects. The highest exposure levels measured with the personal sampling device on the robot in our experiment was 20 ppm for 15 min, which was well below the OSHA PEL of 50 ppm for 8 h.

CONCLUSION

This study demonstrates that it is feasible to evaluate personal exposures from either the area sampling array or the OP-FTIR. The 95% CI of the slopes in our regression models includes 1, although the standard errors were relatively large due to the limited sample size. The fact that the predictability of our estimation approach may depend on which concentration gradient model we adopted, somewhat limits its application. Our proposed approach might be more suitable for evaluating relative exposure, rather than the absolute exposure. This conclusion was supported by the

good Spearman correlation coefficients (0.78–0.81) observed between the true and estimated exposures.

The linear algorithm for $C_{TWAkrig}$ or the Gaussian function for $C_{TWAgauss}$ and $C_{TWAftir}$ generally work well for this type of application. The estimated exposures were higher than the true exposure but had very good correlations. From the viewpoint of protecting workers, this makes our approach more favorable since the estimations have some degree of protection built into the method. The sensitivity and specificity analysis shows that our approach is suitable for use as a warning system and is likely to be highly protective for worker overexposures.

Acknowledgements—We thank Ms Kathy Hall for her assistance with editing the manuscript. This research was partially supported by the National Institute for Occupational and Safety Health (NIOSH) grant RO1OH02660. This does not constitute an endorsement by NIOSH of the views expressed in this article.

REFERENCES

Esler MB, Griffith DWT, Wilson SR *et al*. (2000) Precision trace gas analysis by FT-IR spectroscopy. 2. The C-13/C-12 isotope ratio of CO2. Anal Chem; 72: 216–21.

Fisher L, Van Belle G. (1993) Biostatistics: a methodology for the health sciences. New York: Wiley. ISBN 0471584657.

Haaland DM, Easterling RG. (1982) Application of new least-squares methods for the quantitative infrared analysis of multicomponent samples. Appl Spectrosc; 36: 665–72.

Hashmonay RA. (2001) Use of optical remote sensing devices in determining fugitive emissions. Proceedings of A&WMA's 94th Annual Conference & Exhibition; Orlando, FL.

Hashmonay RA, Yost MG, Wu CF. (1998) Ambient gaseous leak detection using radial scanning computed tomography and optical remote sensing. SPIE environmental monitoring and remediation technologies conference, Boston, MA: SPIE.

Hashmonay RA, Yost MG, Wu CF. (1999) Computed tomography of air pollutants using radial scanning path-integrated optical remote sensing. Atmos Environ; 33: 267–74.

Hennekens CH, Buring JE, Mayrent SL. (1987) Epidemiology in medicine. Boston, MA: Little Brown. ISBN 0316356360.

Levine SP, Ying LS, Strang CR *et al*. (1989) Advantages and disadvantages in the use of fourier transform infrared (FTIR) and filter infrared (FIT) spectrometers for monitoring airborne gases and vapors of industrial hygiene concern. Appl Ind Hyg; 4: 180.

Wu CF. (2002) Applying optical remote sensing techniques to evaluate personal exposure [dissertation]. Department of Environmental Health. University of Washington, Seattle, WA.

Wu CF, Yost MG, Hashmonay RA *et al*. (2004) Applying open-path FTIR with computed tomography to evaluate personal exposures. Part 1: Simulation studies. Ann Occup Hyg; in press.

Wu CF, Yost MG, Hashmonay RA *et al*. (1999) Experimental evaluation of a radial beam geometry for mapping air pollutants using optical remote sensing and computed tomography. Atmos Environ; 33: 4709–16.

Wu CF, Yost MG, Hashmonay RA *et al*. (2003) Path concentration profile reconstruction of optical remote sensing measurements using polynomial curve fitting procedures. Atmos Environ; 37: 1879–88.

Yost MG, Xiao HK, Spear RC *et al*. (1992) Comparative testing of an FTIR remote optical sensor with area samplers in a controlled ventilation chamber. Am Ind Hyg Assoc J; 53: 611–6.